The Journal of Infectious Diseases
MAJOR ARTICLE

Middle East Respiratory Syndrome Coronavirus Causes Multiple Organ Damage and Lethal Disease in Mice Transgenic for Human Dipeptidyl Peptidase 4

Kun Li,[1] Christine Wohlford-Lenane,[1] Stanley Perlman,[1,2,5] Jincun Zhao,[2] Alexander K. Jewell,[1] Leah R. Reznikov,[3] Katherine N. Gibson-Corley,[4] David K. Meyerholz,[4] and Paul B. McCray Jr[1,2]

[1]Department of Pediatrics, [2]Department of Microbiology, [3]Department of Internal Medicine, [4]Department of Pathology, and [5]Interdisciplinary Program in Immunology, University of Iowa, Iowa City

Middle East respiratory syndrome coronavirus (MERS-CoV) causes life-threatening disease. Dipeptidyl peptidase 4 (DPP4) is the receptor for cell binding and entry. There is a need for small-animal models of MERS, but mice are not susceptible to MERS because murine dpp4 does not serve as a receptor. We developed transgenic mice expressing human DPP4 (hDPP4) under the control of the surfactant protein C promoter or cytokeratin 18 promoter that are susceptible to infection with MERS-CoV. Notably, mice expressing hDPP4 with the cytokeratin 18 promoter developed progressive, uniformly fatal disease following intranasal inoculation. High virus titers were present in lung and brain tissues 2 and 6 days after infection, respectively. MERS-CoV–infected lungs revealed mononuclear cell infiltration, alveolar edema, and microvascular thrombosis, with airways generally unaffected. Brain disease was observed, with the greatest involvement noted in the thalamus and brain stem. Animals immunized with a vaccine candidate were uniformly protected from lethal infection. These new mouse models of MERS-CoV should be useful for investigation of early disease mechanisms and therapeutic interventions.

Keywords. transgenic mice; MERS; DPP4/CD26.

Middle East respiratory syndrome (MERS) first emerged on the Saudi Arabian peninsula, in 2012. A new coronavirus, MERS coronavirus (MERS-CoV), was identified as the causative agent [1], and dipeptidyl peptidase 4 (DPP4; CD26) was identified as its receptor [2]. The disease spectrum ranges from asymptomatic cases to acute respiratory distress syndrome, circulatory collapse, multiorgan failure, and death [3]. As of 5 October 2015, the World Health Organization has been notified of 1589 laboratory-confirmed cases of MERS-CoV infection in >24 countries, resulting in at least 567 related deaths. The greatest mortality occurs in elderly individuals and those with comorbidities [4–7].

Epidemiologic studies indicate that MERS-CoV can spread to humans from infected dromedary camels [8]. A closely related virus is resident in wild bats, suggesting that they serve as natural reservoirs for MERS-CoV–like viruses [9]. Although human to human or zoonotic spread of MERS has not reached epidemic or pandemic levels, its potential to spread between persons was demonstrated in healthcare settings in the Middle East [10] and by the recent outbreak in South Korea caused by a single infected individual [11].

Received 25 June 2015; accepted 8 October 2015; published online 20 October 2015.
Correspondence: P. B. McCray, Department of Pediatrics, 6320 PBDB, University of Iowa, Iowa City, IA 52242 (paul-mccray@uiowa.edu).

The Journal of Infectious Diseases® 2016;213:712–22

DOI: 10.1093/infdis/jiv499

MERS-CoV can infect rabbits and camels and some species of nonhuman primates (rhesus macaques and common marmosets [12]). Marmosets are thought to develop a severe progressive lung disease [13], although this has recently been questioned [14]. The other animals develop a milder, self-limited respiratory illness.

Because large-animal and primate studies are resource intensive, a small-animal model is desirable. The MERS-CoV spike (S) glycoprotein does not bind the murine dpp4 protein efficiently, therefore preventing infection [15, 16]. We reported that mice sensitized to MERS-CoV by adenoviral transduction of *hDPP4* to pulmonary epithelia confers productive virus replication, allowing rapid screening of phenotypes in genetically modified mouse strains [17].

A transgenic mouse model would help investigate MERS pathogenesis and aid development of vaccine and antiviral therapies, in part because reagents to study the immune response are widely available. Recently, Agrawal et al described mice expressing a *hDPP4* transgene with the ubiquitous CAGGS promoter (cytomegalovirus immediate-early enhancer and chicken β-actin promoter) [18]. When exposed to MERS-CoV (10^6 50% tissue culture infective doses administered intranasally) these mice exhibited progressive weight loss and died with evidence of high virus titers and inflammatory responses in lung and brain tissues. They detected virus antigen in the heart, spleen, and intestine, indicating spread beyond the lungs and brain. To develop new MERS models, we generated mice expressing hDPP4 in epithelial cells, using 2 different cell type–specific

promoters. We show that transgenic expression of hDPP4 in epithelia facilitates MERS-CoV replication in lung tissue. Depending on the promoter selected, the disease outcome ranged from mild and self-limited to lethal with lung and brain tissue involvement.

METHODS

Generation of Human DPP4 Transgenic Mice

All studies were approved by the Animal Care and Use Committee of the University of Iowa. We used 2 different promoters (cytokeratin 18 or surfactant protein C) to direct hDPP4 expression in epithelia (Figure 1*A* and Supplementary Figure 1*A*). A FLAG epitope–tagged hDPP4 complementary DNA (Origene) was cloned into the pK18mTElacZ-K18i6×7pA vector to create pK18-*hDPP4* [19–21]. The human surfactant protein C (SPC) promoter, a gift from Dr Teodora Georgieva (BIO5 Institute, Tucson, Arizona), was used to generate the pSPC-*hDPP4* vector. Purified DNA fragments from the pK18-*hDPP4* and pSPC-*hDPP4* vectors were injected into pronuclei of fertilized B6SJL (C57BL/6J X SJL/J) mouse eggs to generate transgenic embryos. Mice transgenic for *hDPP4* expression were detected by polymerase chain reaction (PCR), using the following primers: forward, CCA AAG ACT GTA CGG GTT CC; and reverse, CCA AAG CTG AAT TGT CTT CCA G.

Infection of Transgenic Mice With MERS-CoV

The MERS-CoV (EMC2012 strain, passage 8) was provided by Drs Bart Haagmans and Ron Fouchier (Erasmus Medical Center). Virus was propagated and titered by plaque assay on Vero-81 cells. Mice expressing hDPP4 were anesthetized with ketamine/xylazine and infected intranasally with MERS-CoV

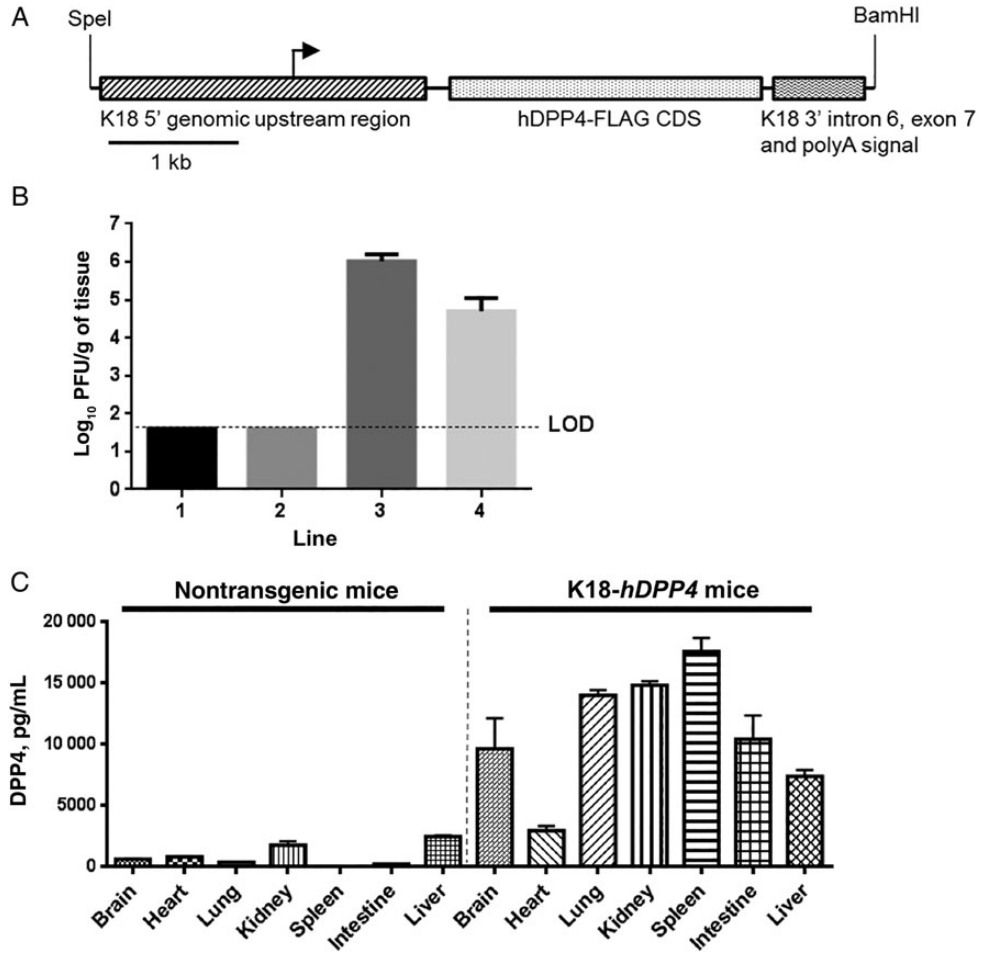

Figure 1. Generation and characterization of K18-*hDPP4* mice. *A*, The hDPP4 coding sequence was cloned into a plasmid containing the 5′ and 3′ genomic regions of human cytokeratin 18 (K18). The K18 5′ genomic region consists of a 2.5-kb upstream genomic sequence, promoter, and first intron of the human K18 gene while the K18 3′ region consists of exon 6, intron 6, exon 7, and approximately 300 base pairs of 3′ untranslated region of the human K18 gene, including the K18 polyA signal. Immediately upstream of the hDPP4 start codon is a translational enhancer (TE) sequence from alfalfa mosaic virus. *B*, Four K18-*hDPP4* transgenic founder lines were generated and intranasally inoculated with 1×10^5 plaque-forming units (PFU) of Middle East respiratory syndrome coronavirus. Lung titers of founder mice were determined by plaque assay 3 days after infection. Data are mean ± standard deviation [SD] for 6–10 mice/line. *C*, Quantitative measurement of human DPP4 concentrations in tissues of nontransgenic or K18-*hDPP4* founder line 3 by enzyme-linked immunosorbent assay. Data are mean ± SD for 3 mice. Abbreviation: LOD, limit of detection.

in 50 μL of Dulbecco's modified Eagle's medium (DMEM). Mice were examined daily and temperatures and weights recorded. Non-transgenic littermates served as controls. MERS-CoV work was conducted in a Biosafety Level 3 (BSL3) Laboratory.

Virus Titers

Tissues were removed aseptically, disassociated with a manual homogenizer in 1X PBS, briefly centrifuged, and supernatants removed. Samples were titered on Vero-81 cells as reported elsewhere [17].

DPP4 Protein Abundance

DPP4 protein abundance was measured by enzyme-linked immunosorbent assay (ELISA; human DPP4 DuoSet [catalog no. DY1180], R&D Systems, Minneapolis, Minnesota) following the manufacturer's protocol.

Extraction of Total RNA and Real-Time Quantitative PCR (qPCR)

Details are available in the Supplementary Materials.

Histologic and Immunohistochemical Analyses

Details are available in the Supplementary Materials.

MERS-CoV Infection of Human Cell Lines and Primary Porcine Astrocytes

The human neuroblastoma cell line SK-N-SH was grown in Roswell Park Memorial Institute 1640 medium with 10% fetal bovine serum (FBS). The glioma cell line U138MG and murine astrocytoma cell line DBT were cultured in DMEM with 10% FBS. Primary porcine glial cells were cultured as previously described [22]. Dissociated cells were allowed to attach to collagen-coated plates and cultured for 2–3 weeks. Cells were infected with MERS-CoV at multiplicity of infection (MOI) of 1. At time 0 and 2 days after infection, supernatants were harvested for titers and cells processed for immunostaining.

Inhibition of MERS-CoV Infection by Passive and Active Immunization

Venezuelan equine encephalitis replicon particles (VRPs) expressing the MERS-CoV S glycoprotein or green fluorescent protein (GFP) were constructed as previously described [17]. cytokeratin 18 (K18)–*hDPP4* transgenic mice were immunized in the foot pad with 1×10^5 infectious units (IU) of VRP-S or VRP-GFP in 20 μL of PBS and boosted with the same doses 4 weeks later. Two weeks after the second immunization, mice received 1×10^5 plaque-forming units (PFU) of MERS-CoV. For passive immunization, nontransgenic mice received 1×10^5 IU of VRP-S or VRP-GFP and then were boosted with the same dose 4 weeks later. Two weeks later, serum was harvested and 300 μL of serum transferred into K18-*hDPP4* mice intraperitoneally 1 day before MERS-CoV infection.

Statistical Analysis

The Student *t* test or analysis of variance with the Dunn multiple comparison test were used to analyze differences in mean values between groups unless otherwise specified. Results are expressed as mean ± standard error or standard deviation, as indicated. *P* values of ≤.05 were considered statistically significant.

RESULTS

Characterization of hDPP4 Transgenic Mice

DPP4 is broadly expressed in human tissues and cells [23]. In primary cell culture and organ culture models, MERS-CoV predominantly infects nonciliated epithelial cell types of the respiratory tract [2, 24]. To direct MERS-CoV receptor expression to pulmonary epithelia, we used the SPC promoter (Supplementary Figure 1*A*) or the K18 promoter (Figure 1*A*) as described in Methods. The SPC promoter drives expression in bronchiolar and alveolar epithelia [25]. In contrast, the *K18* promoter confers transgene expression in airway and alveolar epithelial cells, as well as epithelia of the liver, kidney, and gastrointestinal tract, and some cells of the nervous system [19]. We generated 8 SPC-*hDPP4* founder lines and 4 K18-*hDPP4* founder lines.

We first screened F2 mice from each founder line for evidence of a pulmonary infection following intranasal inoculation with 1×10^5 PFU of MERS-CoV. We identified 3 SPC-*hDPP4* lines (Supplementary Figure 1*B*) and 2 K18-*hDPP4* lines (Figure 1*B*) with productive MERS-CoV infections, based on titers 3 days after infection. The titers achieved in the K18-*hDPP4* lines exceeded those in the SPC-*hDPP4* lines. We selected founder line 3 from both the SPC-*hDPP4* and K18-*hDPP4* lines for additional studies, as these showed the highest virus titers 3 days after infection. Intranasal infection of transgenic mice and their nontransgenic littermates from SPC-*hDPP4* line 3 with MERS-CoV caused no mortality or changes in body temperature, but mice failed to gain weight as compared to nontransgenic littermates (Supplementary Figure 1*C*–*F*). Virus was cleared by 14 days after infection.

MERS-CoV–Infected K18-*hDPP4* Mice Develop Lethal Disease

We detected DPP4 protein expression in brain, heart, lung, kidney, spleen, intestine, and liver of K18-*hDPP4* mice (Figure 1*C*). In contrast to the SPC-*hDPP4* transgenic mice, K18-*hDPP4* mice inoculated intranasally with MERS-CoV uniformly exhibited weight loss and hypothermia, and they died at 6–7 days after infection (Figure 2*A*–*C*). MERS-CoV titers were highest in lung tissue 2 days after infection (6×10^7 PFU/g of tissue) and then declined at 4 and 6 days after infection. In contrast, virus titers in brain were undetectable at 2 days after infection and then increased to 10^5 and 10^8 PFU/g of tissue 4 and 6 days after infection, respectively (Figure 2*D*). Although the K18 promoter is active in the epithelia of multiple organs, no virus was titered from the kidney (Figure 2*D*). We quantified virus RNA distribution in tissues and blood by PCR 2 and 4 days after infection (Figure 2*E*). Virus RNA was abundant in lung 2 and 4 days after infection. RNA was detected in brain tissue 4 days after infection. Lower levels of viral RNA were also

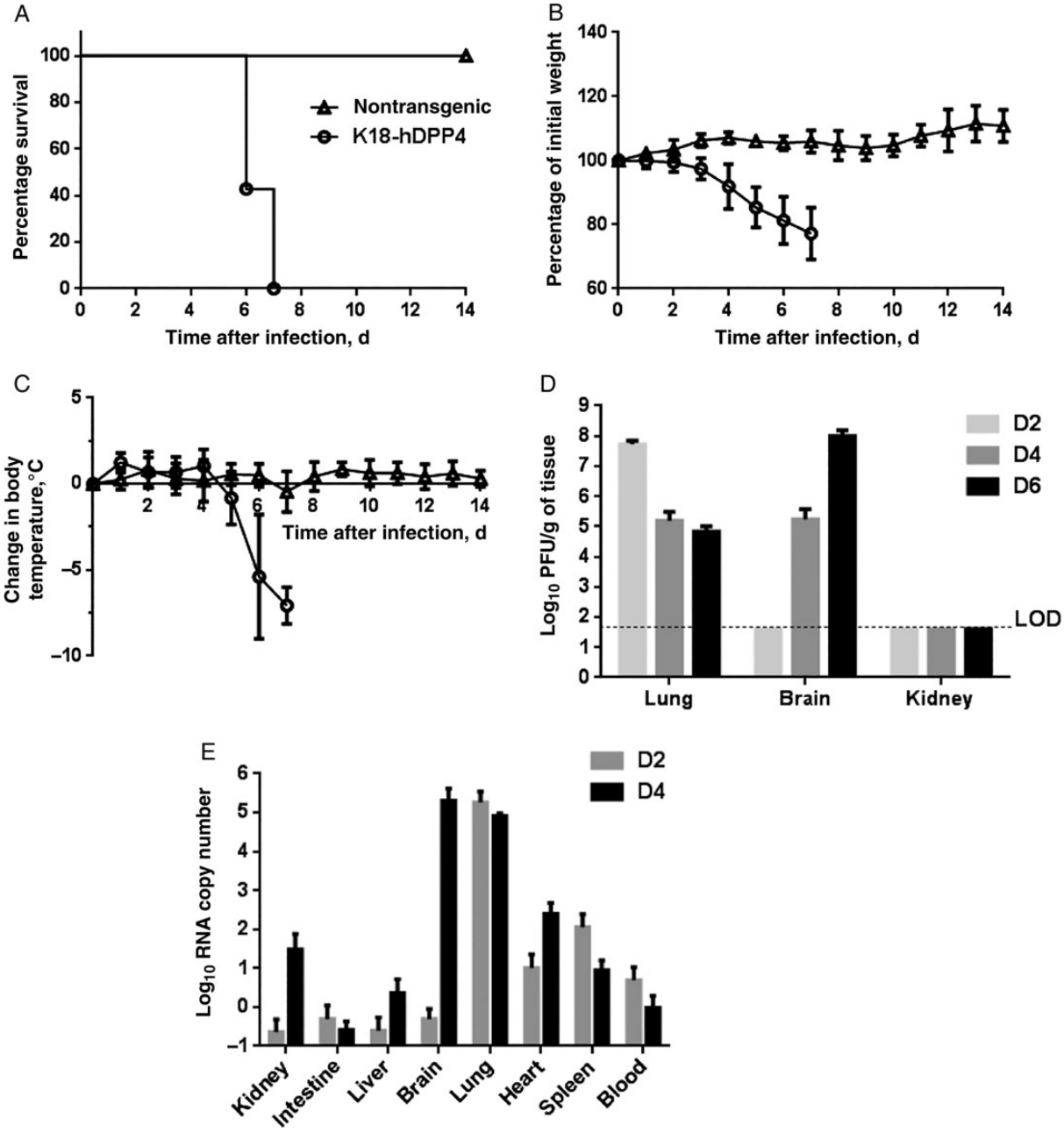

Figure 2. Middle East respiratory syndrome coronavirus (MERS-CoV) infection causes lethal disease in human cytokeratin 18–*hDPP4* mice. *A–C*, Animals were inoculated intranasally with 1×10^5 plaque-forming units (PFU) of MERS-CoV and survival (*A*), weight (*B*), and temperature (*C*) monitored daily. Data are for 4 nontransgenic mice and 14 K18-*hDPP4* mice. *D*, MERS-CoV titers in indicated tissues at days 2, 4, and 6 after infection. Data are for 3–4 mice. *E*, The copy numbers of viral RNA in indicated tissues at days 2 and 4 after infection were analyzed by quantitative real-time polymerase chain reaction targeting regions within open reading frame 1a. Data are for 4 mice. All results are expressed as mean ± SD.

detected in spleen 2 days after infection and in kidney and heart 4 days after infection.

We also asked whether MERS-CoV–infected mice could spread the virus to other animals. MERS-CoV was not transmitted from infected K18-*hDPP4* mice (n = 2) to uninfected K18-*hDPP4* mice (n = 3) housed in the same cages (data not shown). No virus RNA was detected in the brain, lung, or blood of these healthy cohoused mice (data not shown). This was not surprising, however, since mice do not cough or sneeze.

Histopathologic Evaluation of K18-*hDPP4* Lung Tissue Infected With MERS-CoV

MERS-CoV infection in lung was evaluated and scored 2, 4, and 6 days after infection (Table 1). MERS-CoV infection produced

Table 1. Histopathologic Scores of Lung Lesions in Middle East Respiratory Syndrome Coronavirus (MERS-CoV)–Infected Mice

Variable	Uninfected Control Mice, Score, Mean±SEM (n = 4)	MERS-CoV–Infected Mice					
		Day 2 (n = 3)		Day 4 (n = 3)		Day 6 (n = 9)	
		Score, Mean ± SEM	*P* Value[a]	Score, Mean ± SEM	*P* Value[a]	Score, Mean ± SEM	*P* Value[a]
Edema	1 ± 0.0	1 ± 0.0	.999	1.7 ± 0.3	.235	1.6 ± 0.2	.187
Consolidation	1.5 ± 0.3	2.3 ± 0.3	.999	3.0 ± 0.6	.142	3.3 ± 0.2	.004
Cell debris lymphatics	1 ± 0.0	1 ± 0.0	.999	1 ± 0.0	.999	2.1 ± 0.2	.014
Thrombi	1 ± 0.0	1 ± 0.0	.999	2.3 ± 0.3	.027	1.9 ± 0.2	.058
Composite score	1.1 ± 0.1	1.3 ± 0.1	.999	2.0 ± 0.1	.117	2.2 ± 0.1	.002

See "Methods" section for scoring parameters.

Abbreviation: SEM, standard error of the mean.

[a] By the Dunn multiple comparison test, compared with control on day 6.

patchy consolidation (Figure 3*A*) variably composed of cellular inflammation, vascular congestion, and atelectasis. The airways were generally intact, with only scattered, uncommon sloughed cells (Figure 3*B*). In some lungs, lymphatic vessels were filled with degenerative cells and cellular debris (Figure 3*C*). Thrombi (Figure 3*D*) were also observed, with nearby vascular congestion and lesser hemorrhage and necrosis. Alveolar edema was detected in some lung fields (Figure 3*E*). We investigated virus antigen expression in the lungs 2, 4, and 6 days after infection (Supplementary Figure 2). MERS-CoV nucleocapsid (N)

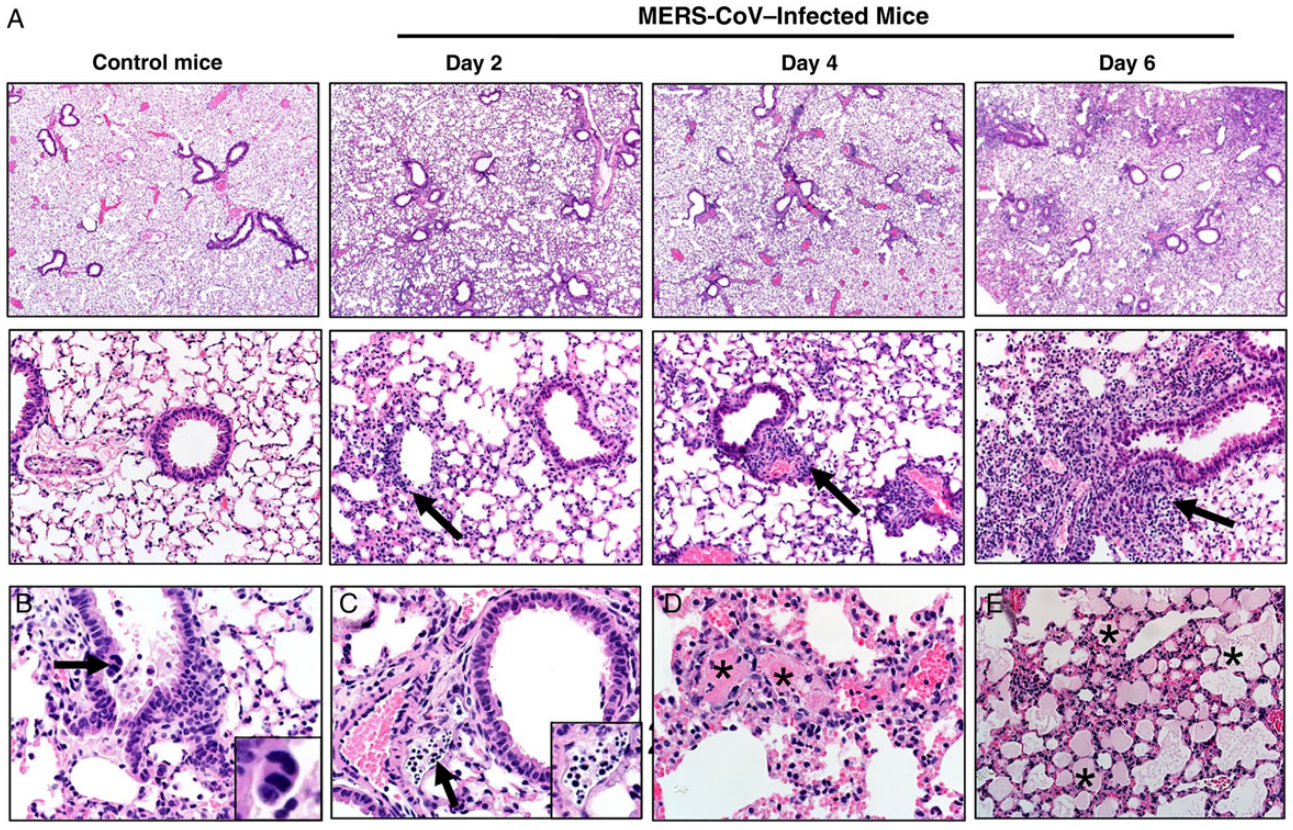

Figure 3. *A*, Lungs from control or Middle East respiratory syndrome coronavirus (MERS-CoV)–infected mice. MERS-CoV infection from days 2, 4, and 6 after infection consistently caused multifocal to patchy consolidation in lung with perivascular and peribronchiolar inflammation (arrows). Section were stained with hematoxylin-eosin (top panels, original magnification ×40; bottom panels, original magnification ×200). *B*, Airways were generally intact, with uncommon scattered sloughed cells (day 6). Note the very rare multinucleate cells (arrow and inset). *C*, Late in the course of infection (day 6), degenerating cells and cellular debris (arrow and inset) could be seen filling several lymphatics. *D*, Vascular thrombi (asterisks) were seen in most cases on days 4 and 6 after infection, with adjacent congestion and lesser amounts of necrosis and hemorrhage. *E*, Edema, characterized by eosinophilic fluid material in airspaces (asterisks), was progressively detected in some cases on days 4 and 6. Section were stained with hematoxylin-eosin (original magnification ×200 [*A*] and ×400 [*B-E*]).

Table 2. Histopathologic Cores in Anatomic Regions of Brain From Middle East Respiratory Syndrome Coronavirus (MERS-CoV)–Infected Mice

	Uninfected Control Mice		MERS-CoV–Infected Mice								
			Day 2			Day 4			Day 6		
Variable	Score, Mean ± SEM	No.	Score, Mean ± SEM	No.	*P* Value[a]	Score, Mean ± SEM	No.	*P* Value[a]	Score, Mean ± SEM	No.	*P* Value[a]
Brain stem	1 ± 0.0	4	1 ± 0.0	3	.999	2.0 ± 0.0	2	.696	4.0 ± 0.0	7	.003
Caudate Putamen	1.0 ± 0.0	3	1.0 ± 0.0	3	.999	1.0 ± 0.0	3	.999	2.2 ± 0.3	6	.054
Cerebellum	1 ± 0.0	4	1 ± 0.0	2	.999	1 ± 0.0	3	.999	1.3 ± 0.3	4	.607
Cerebrum	1 ± 0.0	4	1 ± 0.0	3	.999	1.0 ± 0.0	3	.999	1.8 ± 0.2	8	.035
Ependyma	1.0 ± 0.0	4	1.0 ± 0.0	3	.999	1.0 ± 0.0	3	.999	1.3 ± 0.2	7	.510
Hippocampus	1.0 ± 0.0	2	1.0 ± 0.0	3	.999	1.0 ± 0.0	3	.999	1.4 ± 0.2	9	.581
Olfactory bulb	1.0 ± 0.0	3	NA	. . .		2.0 ± 0.0	1		2.0 ± 0.0	2	
Thalamus	1.0 ± 0.0	4	1.0 ± 0.0	3	.999	2.3 ± 0.3	3	.365	3.4 ± 0.2	7	.004

See "Methods" section for scoring parameters.

Abbreviation: SEM, standard error of the mean.

[a] By the Dunn multiple comparison test, compared with control on day 6.

protein was most abundant in the lung parenchyma in alveolar type I and II cells and in macrophages.

Nervous System Disease in MERS-CoV–Infected K18-*hDPP4* Mice

MERS-CoV was detected at high levels in infected K18-*hDPP4* mice. Transgenic hDPP4 expression in brain was corroborated by ELISA (Figure 1*C*). We evaluated pathologic changes in the brains of MERS-CoV–infected mice 2, 4, and 6 days after infection (Table 2). Compared with controls (Figure 4*A*), MERS-CoV–infected mice exhibited perivascular cuffing (Figure 4*B* and 4*E*), cellular degeneration, and debris (Figure 4*C* and 4*D*) that were absent on day 2, with progressive changes from days 4 to 6 (Table 2). Degenerating and dying neurons sometimes had basophilic cytoplasmic inclusions that were quite prominent (Figure 4*C* and 4*F*) and immunostained for viral antigen (Figure 4*F*). MERS-CoV–induced neuronal lesions were most severe in the thalamus and brain stem (Table 2). More-detailed virus antigen staining in brain tissue 2, 4, 6 days after infection is shown in Supplementary Figure 3. N protein staining was rare 2 and 4 days after infection and principally seen in solitary neurons. In contrast, by 6 days after infection, many neurons were infected. Virus antigen 6 days after infection was preferentially located in the midbrain, thalamus, deep cerebral cortex, and CA2 region of the hippocampus but was uncommon in the cerebellum.

Collectively, these results show that both the lungs and brain developed pathological changes after MERS-COV infection. To differentiate the importance of brain versus lung infection, we used low inoculum doses, to optimize the likelihood that only the brain or the lung would be infected. We used intranasal inocula of 1000, 100, and 10 PFU/animal. Compared with mice receiving a larger inoculum, the onset of weight loss was delayed from 3–4 days after infection to 9–10 days after infection (Figure 4*G*–*I*). Despite this delayed onset of disease signs, 4 of 5 mice died after receipt of the 1000 PFU inoculum, 4 of 5 mice died after receipt of a 100 PFU inoculum, and 3 of 5 mice died following receipt of a 10 PFU inoculum. In a second experiment, MERS-CoV was detected in brain tissue of 3 of 7 mice infected with 10 PFU (approximately 4×10^6 PFU/g of tissue) 9 days after infection. No virus was titered from lung tissue (Figure 4*I*). Thus, mortality correlated with brain infection, suggesting that infection of this organ was most important for the high mortality observed in K18-*hDPP4* mice.

MERS-CoV Infection of Cells From the Nervous System

The clinical course of MERS in severely ill patients sometimes includes neurological manifestations [4, 26], suggesting that MERS-CoV may infect the human central nervous system. Of note, DPP4 is expressed in vascular endothelia and other brain cell types [23, 27–34]. To determine whether MERS-CoV could infect and complete its replication cycle in central nervous system–derived cells, we infected central nervous system–derived human cell lines or primary astrocytes derived from newborn pig brain tissue. Pig cells were previously shown to be permissive to MERS-CoV infection [2]. Human cell lines (U-138 MG and SK-N-SH) and primary porcine astrocytes all expressed DPP4 protein (data not shown). SK-N-SH cells, porcine astrocytes, and control Vero-81 cells supported virus replication (Figure 4*J*), and this result was confirmed by immunostaining for MERS-CoV antigen (Supplementary Figure 3). No human autopsy samples are available to directly assess virus replication in the brain, but these results support the notion that neurological disease is directly virus induced.

Induction of Proinflammatory Cytokines and Chemokines in MERS-CoV–Infected K18-*hDPP4* Mice

Based on studies of cells infected in vitro [35–38], dysregulated cytokine and chemokine production is postulated to contribute to disease severity. We profiled the expression of several

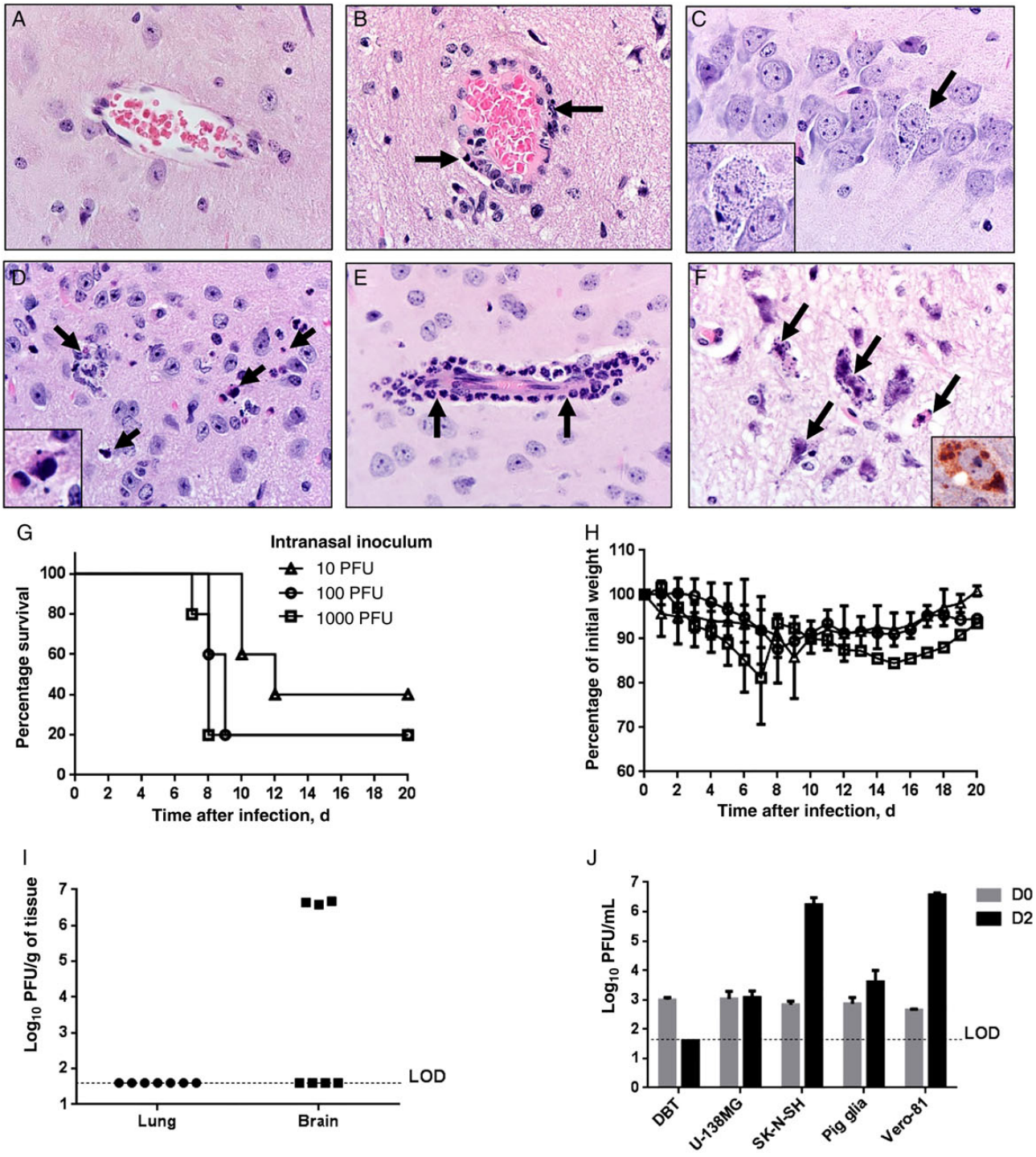

Figure 4. Brain disease in Middle East respiratory syndrome coronavirus (MERS-CoV)–infected human cytokeratin 18 (K18)–*hDPP4* and uninfected mice. *A*, Normal brain from an uninfected mouse. *B*, MERS-CoV caused lymphocytic perivascular cuffing in the infected brain. *C*, Infected neuron in hippocampus 6 days after infection. Note the granular degeneration and basophilic cytoplasmic inclusions (arrow and inset). *D*, Dying cells undergoing degeneration (arrows and inset; 6 days after infection) are detected in highly infected regions such as the thalamus or brain stem. *E*, Meningeal and perivascular cuffing included neutrophilic infiltrates (arrows; 6 days after infection). *F*, Several degenerating cells had small to granular basophilic cytoplasmic inclusions (arrows; 6 days after infection) that were stained with anti–MERS-CoV antibody (inset; brown). Note the neuropil rarefaction. Section were stained with hematoxylin-eosin (original magnification ×600). *G–I*, Outcomes of K18-*hDPP4* mice infected with different intranasal inocula of MERS-CoV. K18-*hDPP4* mice received 1000, 100, or 10 plaque-forming units (PFU) of MERS-CoV and were monitored for survival (*G*) and weight (*H*). There were 5 mice/group. *I*, Lungs and brains of mice receiving 10 PFU were harvested 10 days after inoculation or when they lost 20% of body weight. A total of 3 of 7 MERS-CoV–infected mice showed high virus titers in the brains. *J*, MERS-CoV replicates in cells of the nervous system. Human central nervous system–derived cell lines (U-138 MG an SK-N-SH), primary porcine astrocytes, a murine astrocytoma cell line (DBT), and African green monkey kidney cells (Vero-81) were infected with MERS-CoV at a multiplicity of infection of 1. Titers from these cells immediately after infection (day 0) or 2 days after infection were determined by plaque assay. Data are mean ± SD for 3 replicates/condition. Abbreviation: LOD, limit of detection.

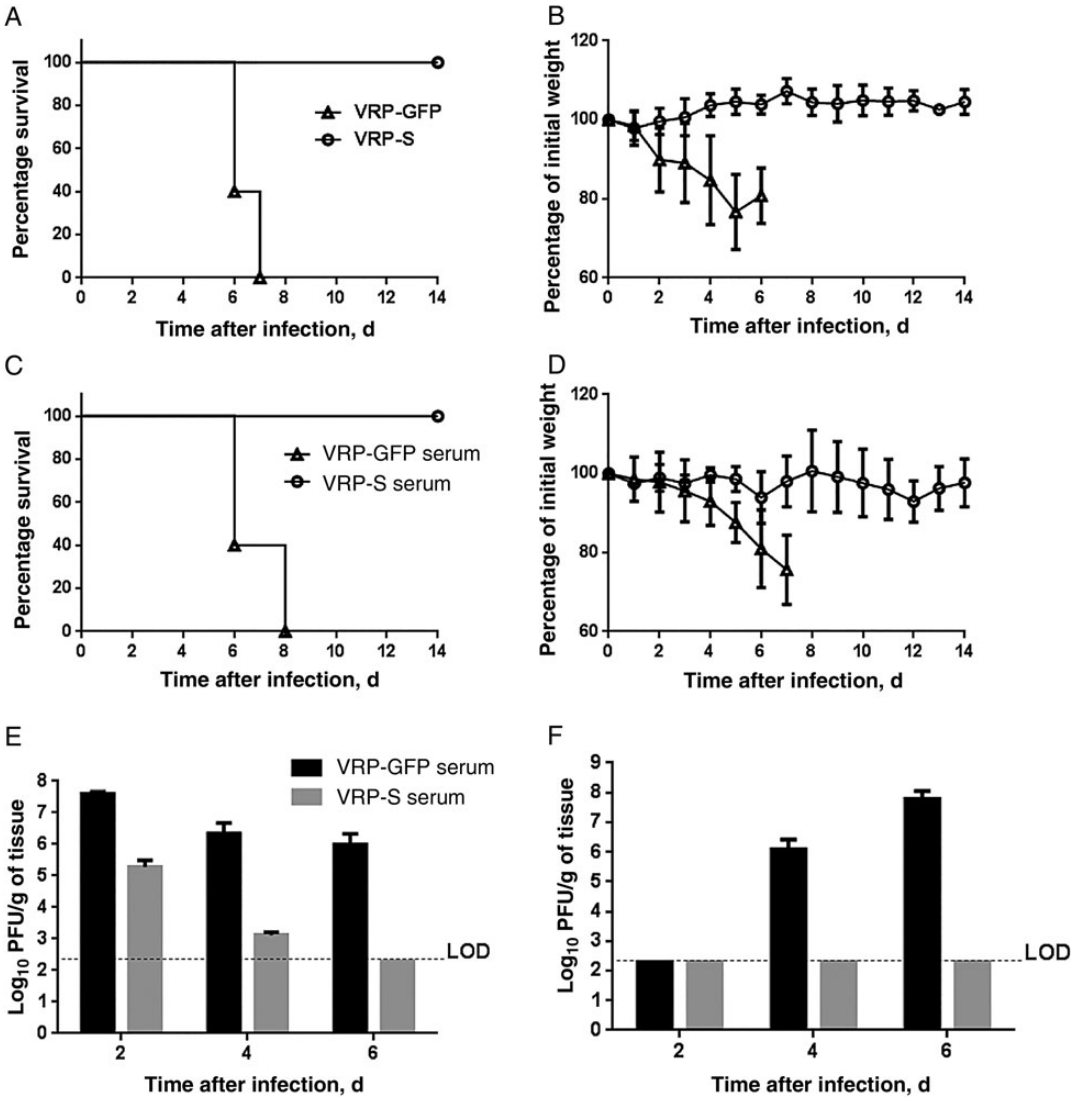

Figure 5. Immunization with Venezuelan equine encephalitis replicon particles (VRPs) expressing Middle East respiratory syndrome coronavirus (MERS-CoV) spike glycoprotein (VRP–MERS-S) or passive immunization protects human cytokeratin 18 (K18)–*hDPP4* mice against MERS-CoV infection. *A* and *B*, K18-*hDPP4* mice were immunized with 1×10^5 infectious units (IU) of VRPs expressing green fluorescent protein (VRP-GFP) or VRP-MERS-S in the footpad and boosted with the same dose 4 weeks later. Mice were infected with 1×10^5 plaque-forming units of MERS-CoV 2 weeks after the boost. *C* and *D*, For passive immunization, nontransgenic mice were immunized as described above. Sera were obtained 2 weeks after boosting and transferred into K18-*hDPP4* mice intraperitoneally 1 day before infection with MERS-CoV. Survival and weights were recorded for active immunization (*A* and *B*) and passive immunization (*C* and *D*). Data are mean ± standard deviation (SD) for 5 mice/group. *E* and *F*, MERS-CoV titers in lung tissue (*E*) and brain tissue (*F*) 2, 4, and 6 days after infection in mice with or without passive immunization. Data are mean ± SD for 3 mice/group. Abbreviation: LOD, limit of detection.

cytokine, chemokine, and antiviral gene products in lung and brain tissues 2, 4, and 6 days after infection, using real-time qPCR. As shown in Supplementary Figure 4, we observed an overall trend that these host defense gene products were first induced in the lung, followed by a later increase in signal in the brain. In the lung, there were significant increases in type I, II, and III interferons by 2 days after infection. The induction of interferon λ in lung was especially remarkable. Upregulation of all classes of interferons occurred later in brain tissue and did not reach the same levels as in lung, with the exception of interferon γ. Several other gene products were increased early in the lung, including ISG15, interleukin 6, interleukin 12p40, interleukin 15, CCL2, CXCL9, and CXCL10. Peak expression of RIG-I, MDA5, PKR, MYD88, tumor necrosis factor α, interleukin 1β, CCL2, CCL5, and CXCL10 was greater in the brain than in the lung at the later time points.

Kidneys From MERS-CoV–Infected Mice

Renal failure is commonly seen in patients with MERS but it is not known whether the kidney is infected by the virus. MERS-CoV–infected mice had scattered-to-patchy evidence of tubular injury, including tubular dilation, cell sloughing/debris, and

cellular necrosis (Supplementary Figure 5). These changes were principally seen late in the course of infection (6 days after infection; 9 of 9 cases) and otherwise only seen rarely/focally at 4 days after infection (3 of 3 cases) and not detected 2 days after infection (0 of 3 cases). Consistent with published results [18], no virus was detected in the kidneys of MERS-CoV–infected animals 2, 4, or 6 days after infection. These pathologic changes are most consistent with shock or hypoxia.

Active or Passive Immunization of K18-*hDPP4* Mice Prevents Clinical Disease

To determine whether K18-*hDPP4* mice will be useful for evaluating anti-MERS-CoV vaccines or therapies, we vaccinated K18-*hDPP4* mice with VRPs expressing the MERS-CoV surface S glycoprotein (VRP-S) or VRP-GFP prior to MERS-CoV infection. Following a primary and secondary immunization, mice were challenged with 1×10^5 PFU of MERS-CoV intranasally. As shown in Figure 5*A* and 5*B*, immunized mice were completely protected against lethal infection. Mice immunized with VRP-S showed 100% survival and no weight loss during the 14-day experiment.

Next, animals were pretreated with serum from mice immunized with VRP-S or VRP-GFP. Intraperitoneal administration of serum from mice immunized with VRP-S 1 day prior to MERS-CoV infection completely prevented the lethal disease manifestations in K18-*hDPP4* mice, including weight loss and clinical disease (Figure 5*C* and 5*D*). Control anti-GFP sera–treated mice all died. We also assessed tissue titers in MERS-CoV–infected mice following passive immunization 2, 4, and 6 days after infection. We observed an accelerated reduction in lung tissue titers in immunized mice, with no virus titered >4 days after infection (Figure 5*E*). Passive immunization completely prevented spread of infection to the brain (Figure 5*F*).

DISCUSSION

The recent outbreak in South Korea demonstrates that MERS-CoV continues to pose significant risks to human health [11]. Here we report new mouse models of MERS-CoV infection. Because the restriction in infecting mouse cells with MERS-CoV is at the level of the receptor [15, 16], we generated mice expressing human DPP4 under control of the SPC or K18 promoters. When challenged with MERS-CoV, a fatal disease course ensued in K18-*hDPP4* mice, with inflammatory disease involving lung and brain tissues. In this setting of severe disease, immunization with VRPs expressing the MERS-CoV S glycoprotein conferred protective immunity. SPC-*hDPP4* mice exhibited a milder disease phenotype. These transgenic mice provide new models for investigation of MERS-CoV infection and the evaluation of therapeutic interventions.

Several animal species have been tested for their susceptibility to MERS-CoV respiratory infection and disease. Mice [39], Syrian hamsters [40], and ferrets [41] do not support MERS-CoV replication. In contrast, rhesus macaques [42, 43], marmosets [13], rabbits [44], and camels [45] all allow the virus to complete its replication cycle. While marmosets develop significant lung pathology with associated mortality when given a large inoculum [13], others report minimal disease in marmosets [14]. The phenotypes in other mammals studied are mild and do not recapitulate a severe MERS-like disease.

Zhao et al reported the first mouse model of MERS infection [17]. They sensitized mice to MERS-CoV infection by delivering adenovirus vectors expressing hDPP4 to the lungs of mice. However, only the lung expressed hDPP4, so virus replication in other organs could not be evaluated. Agrawal et al expressed *hDPP4* behind a universally expressed promoter [18]. Here we expanded the available mouse models by stably expressing *hDPP4* with the SPC and K18 promoters. Both of these promoters exhibit more-restricted expression than the CAGGs promoter used by Agrawal et al [18]. The disease phenotype of the K18-*hDPP4* mice shares many features with the results reported by Agrawal et al [18], including fatal disease, with lung and brain involvement. In contrast, the SPC-*hDPP4* line demonstrated lower lung tissue viral loads than Ad-*hDPP4*–sensitized mice [17], without spread to other organs or associated mortality. This suggests that, with infection restricted to the lung, mouse innate immunity may successfully overcome virulence factors expressed by MERS-CoV and prevent a lethal outcome. A mouse-adapted MERS-CoV strain may help overcome this limitation.

The K18-*hDPP4* transgenic mice developed several disease features of interest. Analysis of the lungs 2, 4, and 6 days after infection revealed ongoing virus replication and significant parenchymal involvement. In addition, the airways exhibited rare sloughed cells, and cell debris was observed within lymphatic vessels. These changes were associated with increases in levels of several innate immune molecules and cytokines, including type I, II, and III interferons; ISG15, interleukin 6, interleukin 12p40, interleukin 15, CCL2, CXCL9, and CXCL10. Interestingly, the level of interferon λ, the predominant mucosal interferon in the lung [46], was markedly induced in the lung of MERS-CoV–infected mice. These lung disease features provide several quantitative end points for evaluation of the efficacy of antiviral therapies.

We previously used the K18 promoter to generate mice transgenic for human ACE2 as a model for severe acute respiratory syndrome (SARS)–CoV infection [21]. Following infection with the Urbani strain of SARS-CoV, K18-*hACE2* mice developed a lethal disease featuring both lung and brain involvement. SARS-CoV spread from the olfactory bulb to primary, secondary, and more-distal connections very rapidly, resulting in lethality. In the present study, the temporal course of brain tissue infection also suggested retrograde virus spread from olfactory neurons. While susceptibility to brain infection sets a high bar for

evaluating new therapies for MERS-CoV infection, we demonstrated the utility of the model for vaccine testing. We acknowledge that high-titer replication and death from central nervous system disease in K18-*hDPP4* transgenic mice may complicate the study of some vaccines and other therapeutic interventions, especially for drugs that do not cross the blood-brain barrier.

The K18-*hDPP4* mice developed lethal disease, with encephalitis contributing to their demise. Is the brain infection in a mouse model of MERS relevant to the disease in humans? We note that DPP4 is expressed in the brains of humans and other mammals [23, 27–34]. We found that MERS-CoV infects human nervous system–derived cell lines and primary porcine astrocytes. It is possible that if MERS-CoV gains access to the human central nervous system, through disruption of the blood brain barrier, via lymphatics [47], or other routes, there are cells expressing DPP4 that could support virus replication. Current knowledge is limited by the absence of any published postmortem data from persons dying from MERS. Interestingly, Arabi et al recently described 3 patients with MERS who had severe neurologic manifestations, including altered consciousness and diffuse brain abnormalities on magnetic resonance imaging involving the white matter and subcortical areas of the frontal, temporal, and parietal lobes, the basal ganglia, and the corpus callosum [26]. While there are many reasons that severely ill patients with MERS might manifest neurologic signs and symptoms, this report indicates that MERS can be associated with progressive neurological manifestations. Further data are needed to understand whether some patients with MERS have central nervous system involvement with infection.

In summary, these MERS mouse models provide a resource for the investigation of early disease mechanisms and therapeutic interventions and provide an economic alternative to other available models of MERS-CoV infection.

Supplementary Materials

Supplementary materials are available at http://jid.oxfordjournals.org. Consisting of data provided by the author to benefit the reader, the posted materials are not copyedited and are the sole responsibility of the author, so questions or comments should be addressed to the author.

Notes

Acknowledgments. We thank Sateesh Krishnamurthy, Jennifer Bartlett, and Patrick Sinn, for careful review of the manuscript; and Jim Hu, for providing the K18 plasmid construct.

Financial support. This work was supported by the National Institutes of Health (NIH; grant PO1 AI060699), the Cell Morphology Core and Pathology Core, supported in part by the Center for Gene Therapy for Cystic Fibrosis, through the NIH (grant P30 DK-54759), and by the Cystic Fibrosis Foundation; the Transgenic Mouse Facility, supported in part by the College of Medicine and by the Center for Gene Therapy for Cystic Fibrosis; and the Roy J. Carver Charitable Trust (to P. B. M.).

Potential conflicts of interest. All authors: No reported conflicts. All authors have submitted the ICMJE Form for Disclosure of Potential Conflicts of Interest. Conflicts that the editors consider relevant to the content of the manuscript have been disclosed.

References

1. Zaki AM, van Boheemen S, Bestebroer TM, Osterhaus AD, Fouchier RA. Isolation of a novel coronavirus from a man with pneumonia in Saudi Arabia. N Engl J Med **2012**; 367:1814–20.
2. Raj VS, Mou H, Smits SL, et al. Dipeptidyl peptidase 4 is a functional receptor for the emerging human coronavirus-EMC. Nature **2013**; 495:251–4.
3. Zumla AI, Hui DS, Perlman S. Middle East respiratory syndrome. Lancet **2015**; 386:995–1007.
4. Saad M, Omrani AS, Baig K, et al. Clinical aspects and outcomes of 70 patients with Middle East respiratory syndrome coronavirus infection: a single-center experience in Saudi Arabia. Int J Infect Dis **2014**; 29:301–6.
5. Arabi YM, Arifi AA, Balkhy HH, et al. Clinical course and outcomes of critically ill patients with Middle East respiratory syndrome coronavirus infection. Ann Intern Med **2014**; 160:389–97.
6. Kapoor M, Pringle K, Kumar A, et al. Clinical and laboratory findings of the first imported case of Middle East respiratory syndrome coronavirus to the United States. Clin Infect Dis **2014**; 59:1511–8.
7. Al-Hameed F, Wahla AS, Siddiqui S, et al. Characteristics and outcomes of Middle East respiratory syndrome coronavirus patients admitted to an intensive care unit in Jeddah, Saudi Arabia. J Intensive Care Med **2015**; doi:10.1177/0885066615579858.
8. Azhar EI, El-Kafrawy SA, Farraj SA, et al. Evidence for camel-to-human transmission of MERS coronavirus. N Engl J Med **2014**; 370:2499–505.
9. Corman VM, Ithete NL, Richards LR, et al. Rooting the phylogenetic tree of middle East respiratory syndrome coronavirus by characterization of a conspecific virus from an African bat. J Virol **2014**; 88:11297–303.
10. Assiri A, McGeer A, Perl TM, et al. Hospital outbreak of Middle East respiratory syndrome coronavirus. N Engl J Med **2013**; 369:407–16.
11. Hui DS, Perlman S, Zumla A. Spread of MERS to South Korea and China. Lancet Respir Med **2015**; 3:509–10.
12. Sutton TC, Subbarao K. Development of animal models against emerging coronaviruses: From SARS to MERS coronavirus. Virology **2015**; 479–480C:247–58.
13. Falzarano D, de Wit E, Feldmann F, et al. Infection with MERS-CoV causes lethal pneumonia in the common marmoset. PLoS Pathog **2014**; 10:e1004250.
14. Johnson RF, Via LE, Kumar MR, et al. Intratracheal exposure of common marmosets to MERS-CoV Jordan-n3/2012 or MERS-CoV EMC/2012 isolates does not result in lethal disease. Virology **2015**; 485:422–30.
15. van Doremalen N, Miazgowicz KL, Milne-Price S, et al. Host species restriction of Middle East respiratory syndrome coronavirus through its receptor, dipeptidyl peptidase 4. J Virol **2014**; 88:9220–32.
16. Barlan A, Zhao J, Sarkar MK, et al. Receptor variation and susceptibility to Middle East respiratory syndrome coronavirus infection. J Virol **2014**; 88:4953–61.
17. Zhao J, Li K, Wohlford-Lenane C, et al. Rapid generation of a mouse model for Middle East respiratory syndrome. Proc Natl Acad Sci U S A **2014**; 111:4970–5.
18. Agrawal AS, Garron T, Tao X, et al. Generation of transgenic mouse model of Middle East Respiratory Syndrome-Coronavirus infection and disease. J Virol **2015**; 89:3659–70.
19. Chow YH, Plumb J, Wen Y, et al. Targeting transgene expression to airway epithelia and submucosal glands, prominent sites of human CFTR expression. Mol Ther **2000**; 2:359–67.
20. Chow YH, O'Brodovich H, Plumb J, et al. Development of an epithelium-specific expression cassette with human DNA regulatory elements for transgene expression in lung airways. Proc Natl Acad Sci U S A **1997**; 94:14695–700.
21. McCray PB Jr, Pewe L, Wohlford-Lenane C, et al. Lethal infection of K18-hACE2 mice infected with severe acute respiratory syndrome coronavirus. J Virol **2007**; 81:813–21.
22. Reznikov LR, Dong Q, Chen JH, et al. CFTR-deficient pigs display peripheral nervous system defects at birth. Proc Natl Acad Sci U S A **2013**; 110:3083–8.
23. Lambeir AM, Durinx C, Scharpe S, De Meester I. Dipeptidyl-peptidase IV from bench to bedside: an update on structural properties, functions, and clinical aspects of the enzyme DPP IV. Crit Rev Clin Lab Sci **2003**; 40:209–94.
24. Chan RW, Chan MC, Agnihothram S, et al. Tropism of and innate immune responses to the novel human betacoronavirus lineage C virus in human ex vivo respiratory organ cultures. J Virol **2013**; 87:6604–14.
25. Glasser SW, Korfhagen TR, Wert SE, et al. Genetic element from human surfactant protein SP-C gene confers bronchiolar-alveolar cell specificity in transgenic mice. Am J Physiol **1991**; 261:L349–56.
26. Arabi YM, Harthi A, Hussein J, et al. Severe neurologic syndrome associated with Middle East respiratory syndrome corona virus (MERS-CoV). Infection **2015**; 43:495–501.
27. Barnes K, Kenny AJ, Turner AJ. Localization of aminopeptidase N and dipeptidyl peptidase IV in pig striatum and in neuronal and glial cell cultures. Eur J Neurosci **1994**; 6:531–7.

28. Schnabel R, Bernstein HG, Luppa H, Lojda Z, Barth A. Aminopeptidases in the circumventricular organs of the mouse brain: a histochemical study. Neuroscience **1992**; 47:431–8.
29. Bourne A, Barnes K, Taylor BA, Turner AJ, Kenny AJ. Membrane peptidases in the pig choroid plexus and on other cell surfaces in contact with the cerebrospinal fluid. Biochem J **1989**; 259:69–80.
30. Mitro A, Lojda Z. Histochemistry of proteases in ependyma, choroid plexus and leptomeninges. Histochemistry **1988**; 88:645–6.
31. Mentzel S, Dijkman HB, Van Son JP, Koene RA, Assmann KJ. Organ distribution of aminopeptidase A and dipeptidyl peptidase IV in normal mice. J Histochem Cytochem **1996**; 44:445–61.
32. Busek P, Stremenova J, Sedo A. Dipeptidyl peptidase-IV enzymatic activity bearing molecules in human brain tumors–good or evil? Front Biosci **2008**; 13:2319–26.
33. Busek P, Stremenova J, Krepela E, Sedo A. Modulation of substance P signaling by dipeptidyl peptidase-IV enzymatic activity in human glioma cell lines. Physiol Res **2008**; 57:443–9.
34. Stremenova J, Krepela E, Mares V, et al. Expression and enzymatic activity of dipeptidyl peptidase-IV in human astrocytic tumours are associated with tumour grade. Int J Oncol **2007**; 31:785–92.
35. Selinger C, Tisoncik-Go J, Menachery VD, et al. Cytokine systems approach demonstrates differences in innate and pro-inflammatory host responses between genetically distinct MERS-CoV isolates. BMC Genomics **2014**; 15:1161.
36. Scheuplein VA, Seifried J, Malczyk AH, et al. High secretion of interferons by human plasmacytoid dendritic cells upon recognition of Middle East Respiratory Syndrome Coronavirus. J Virol **2015**; 89:3859–69.
37. Zhou J, Chu H, Li C, et al. Active replication of Middle East respiratory syndrome coronavirus and aberrant induction of inflammatory cytokines and chemokines in human macrophages: implications for pathogenesis. J Infect Dis **2014**; 209: 1331–42.
38. Chu H, Zhou J, Wong BH, et al. Productive replication of Middle East respiratory syndrome coronavirus in monocyte-derived dendritic cells modulates innate immune response. Virology **2014**; 454–455:197–205.
39. Coleman CM, Matthews KL, Goicochea L, Frieman MB. Wild-type and innate immune-deficient mice are not susceptible to the Middle East respiratory syndrome coronavirus. J Gen Virol **2014**; 95:408–12.
40. de Wit E, Prescott J, Baseler L, et al. The Middle East respiratory syndrome coronavirus (MERS-CoV) does not replicate in Syrian hamsters. PLoS One **2013**; 8: e69127.
41. Raj VS, Smits SL, Provacia LB, et al. Adenosine deaminase acts as a natural antagonist for dipeptidyl peptidase 4-mediated entry of the Middle East respiratory syndrome coronavirus. J Virol **2014**; 88:1834–8.
42. de Wit E, Rasmussen AL, Falzarano D, et al. Middle East respiratory syndrome coronavirus (MERS-CoV) causes transient lower respiratory tract infection in rhesus macaques. Proc Natl Acad Sci U S A **2013**; 110:16598–603.
43. Munster VJ, de Wit E, Feldmann H. Pneumonia from human coronavirus in a macaque model. N Engl J Med **2013**; 368:1560–2.
44. Haagmans BL, van den Brand JM, Provacia LB, et al. Asymptomatic Middle East respiratory syndrome coronavirus infection in rabbits. J Virol **2015**; 89:6131–5.
45. Adney DR, van Doremalen N, Brown VR, et al. Replication and shedding of MERS-CoV in upper respiratory tract of inoculated dromedary camels. Emerg Infect Dis **2014**; 20:1999–2005.
46. Jewell NA, Cline T, Mertz SE, et al. Lambda interferon is the predominant interferon induced by influenza A virus infection in vivo. J Virol **2010**; 84:11515–22.
47. Louveau A, Smirnov I, Keyes TJ, et al. Structural and functional features of central nervous system lymphatic vessels. Nature **2015**; 523:337–41.